Proceedings of IMECE'03
2003 ASME International Mechanical Engineering Congress
Washington, D.C., November 15–21, 2003

IMECE2003-41493

DYNAMIC MODELING AND DESIGN OF A HIGH FREQUENCY MICRO VACUUM PUMP

Aaron Astle
Department of Aerospace Engineering
University of Michigan

Luis P. Bernal
Department of Aerospace Engineering
University of Michigan

Peter Washabaugh
Department of Aerospace Engineering
University of Michigan

Hanseup Kim
Electrical Engineering and Computer Sciences Department
University of Michigan

Khalil Najafi
Electrical Engineering and Computer Science Department
University of Michigan

ABSTRACT

A dynamic model of MEMS-fabricated multistage micro vacuum pumps for use in a highly-integrated chemical monitoring system is described. A thermodynamic analysis shows that in order to meet the performance requirements of the system, the micro pump must be operated at very high frequency of approximately 50 kHz. At these frequencies, dynamic effects and resonances due to the interaction of the valves and the pump cavities can play an important limiting role in pump performance. Dynamical effects can also increase the pressure difference between pump cavities increasing the required actuation voltage. The present dynamic model uses integral forms of the momentum and mass conservation equations. Key components of the model are the viscous and inertial terms of the pump's "checkerboard" microvalves, which are evaluated using a CFD model of the valves. At low frequencies, the model results show increased mass flow rate with increased frequency in good agreement with a thermodynamic model. Maximum performance is reached at frequencies of the order of the resonant frequency of the micro pump. The model is also used to study the effect of valve timing and operating point on mass flow rate and power consumption at high frequency.

1 INTRODUCTION

We report the results of a dynamic model developed to determine the high frequency performance of a MEMS-fabricated multi-stage vacuum pump. Astle *et al.*[1] describe the design and operational characteristics of a multistage gas micropump for use in a micro gas chromatograph (μGC). The micro vacuum pump performance requirements are dictated by the sensitivity and fluidic layout of the gas chromatograph, which determine the flow rate and pressure rise that the pump must deliver. The micro gas chromatograph has two operating modes: the sampling mode and the analysis mode. During sampling the pump must deliver a relatively large mass flow rate with a low pressure rise. During analysis the gas is pumped through the chromatograph column and the micropump must deliver a relatively low mass flow rate with a higher pressure rise. Small size and low power consumption are also important considerations in the present application. Astle *et al.*[1] proposed a multi stage electrostatically actuated micro vacuum pump and showed that micro gas chromatograph requirements can be met by operating the pump at a very high frequency. Thus the present investigation was initiated to determine the pump performance at high frequencies.

A number of micropump designs have been reported in the literature for gas pumping applications. Zengerle & Sandmaier[2] provide an overview of early developments of micropumps. A common feature found in most of the designs is that the mass flow rate varies dramatically as the operating frequency is changed. The design of Koch *et al.*[3] shows a maximum flow rate at a few hundred Hertz followed by a rapid decrease of the flow rate as the frequency is increased. Stehr *et al.*[4] report a change from 1000 μl/min at 50 Hz to negative 800μl/min at 140 Hz for a VAMP micropump. Wijngaart *et al.*[5] show that for a valve-less micropump design the flow direction changes at a frequency of a few hundred Hertz. Limited insight on the fundamental mechanisms responsible for this

behavior has been provided. Clearly, these results indicate that a better understanding of dynamic effects of the gas flow in the micropump is required in order to obtain reliable predictions of pump performance. This is the main goal of the present investigation.

The dynamic model discussed here is based on the model of acoustic jets proposed by Müller *et al.*[6,7] which was validated in recent tests[8] at Reynolds and Stokes numbers typical of micro devices. As discussed below the present model is a reduced-order model that describes the pressure in the cavities, and the mass flow through the valves as a function of time for varying frequency. It takes into account compressibility of the gas in the cavities, but ignores compressibility of the flow through the valves since the Mach number is very low. The present analysis ignores nonlinear terms and models viscous and inertia effects using effective viscous and inertial lengths. Estimates of these parameters are obtained from simplified, but geometrically accurate, CFD models of the flow through the valves.

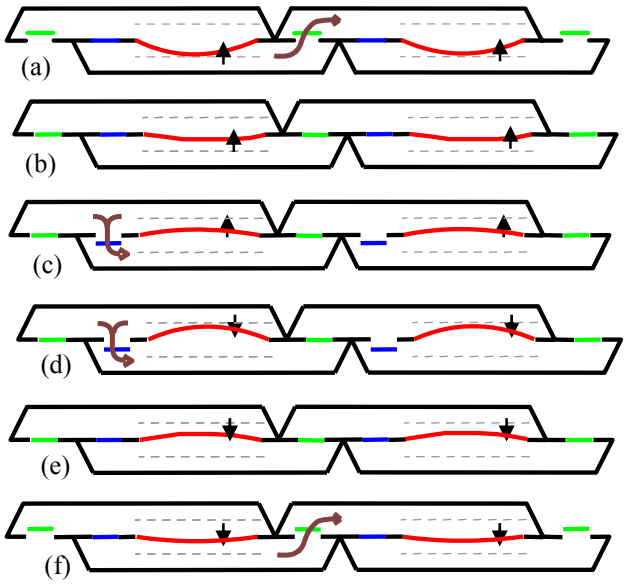

Figure 1. Schematic showing the various states of operation in the multistage micropump. (a) The BT valve open past TDC until t_{cl}/T. (b) Compression of top cavities (c) Gas transfer from top to bottom cavities. (d) TB valve open past TDC until t_{cl}/T. (e) Compression of top cavities (f) Gas transfer from bottom to top cavities.

The operation of a multistage micro vacuum pump is illustrated in Figs. 1 and 2, and discussed by Astle *et al.*[1] Several states in the pumping cycle are shown in Fig. 1, and the timing diagram is shown in Fig. 2. The operation of the pump can be divided into two phases, a “gas pumping” phase and a “gas transfer” phase. During the gas pumping phase the valves are closed and the motion of the membrane compresses or expands air in the cavities. During the gas transfer phase the valves are opened and gas is transferred from one cavity to the next. Clearly the valves should open only when the pressure in the cavities directs the flow from the input to the output. These processes are illustrated in Fig. 1. From a performance point of view, it seems that the unsteady viscous flow through the valves would ultimately limit the amount of gas transferred between cavities. Furthermore the valve timing could also be important particularly at high frequency since the flow in the valves might not be in phase with the membrane motion. In this paper these effects are investigated in a two-stage micro vacuum pump. It is believed that the simpler two-stage micro pump configuration captures the essential features of the 18-stage micropump proposed for the micro gas chromatograph.[1]

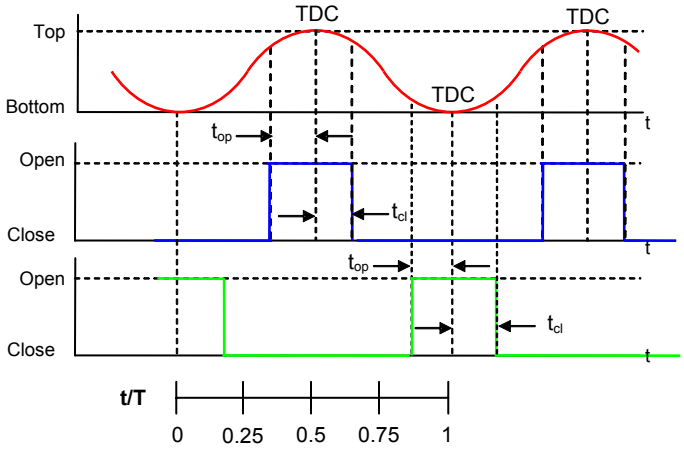

Figure 2. Timing diagram of a multistage micropump. The top trace shows the position of the pumping membrane. The middle trace shows the state of the TB valves. The lower trace shows the state of the BT valves. A normalized cycle time is displayed for reference.

2 NOMENCLATURE

A_E	Effective area of the valve exit
ATDC	After Top Dead Center
BT	Bottom to Top (valve)
BTDC	Before Top Dead Center
C_D	Flow coefficient associated with streamline curvature at the exit plane of the valve
f	Frequency
f_o	Acoustic resonator resonance frequency
H_x	Valve position function for valve x
hg	Height of the valve gap
h_T	Equivalent valve throat height
L_E	Equivalent inertial length of the valve
L_V	Equivalent viscous length of the valve
n	Polytropic gas constant
P_{vac}	Vacuum pressure differential
$\Delta P = P_1 - P_2$	Relative pressure between the pump cavities
Q	Volume flow rate
TB	Top to Bottom (valve)
TDC	Top Dead Center (membrane at electrode)
u_e	Mass average velocity at the exit plane of the valve
V	Total cavity volume
V_r	Compression ratio V_{MIN} /V_{MAX}
α	Speed of sound in the gas

γ	Ratio of specific heats
μ	Dynamic viscosity
ρ	Density

3 DYNAMIC MODEL

The concepts of an acoustic resonator, discussed by Müller *et al.*[6,7], are used to develop a reduced order model of pump performance. The acoustic resonator model assumes that the acoustic wavelength is large compared to the size of the pump cavity. This implies that pressure and density are uniform inside the pump cavities. The flow through the valves determines the damping and inertial effects of the pump system. Figure 3 shows an arrangement of two adjacent pump cavities. This arrangement is the basic unit of the multistage micropump. Equations for the pump system are obtained by taking the line integral of the momentum equation along a streamline from one cavity to the next. The streamline must pass through a microvalve. The momentum equation relates the valve mass average exit velocity to the pressure in the adjacent cavities.

To illustrate the derivation of the model, Fig. 3 shows a streamline originating in cavity 1 and terminating in cavity 2. Writing the incompressible integral from of the momentum equation along this streamline yields:

$$\rho\frac{d}{dt}\int\vec{u}\cdot d\vec{s}+\rho\int\nabla\left[\frac{\vec{u}^2}{2}+\frac{P}{\rho}\right]\cdot d\vec{s}=-\mu\int\left(\nabla\wedge\vec{\omega}\right)\cdot d\vec{s} \qquad (1)$$

which can be written as

$$\frac{du_e}{dt}=\frac{1}{L_E}\frac{\Delta P}{\rho}-\frac{u_e^{\,2}}{2C_D L_E}-8\frac{\mu}{\rho}\frac{u_e}{h_T^{\,2}}\frac{L_V}{L_E}\ , \qquad (2)$$

where u_e is positive in the outward normal direction from the valve exit plane. To simplify the model we assume that second order terms will be small. In this case the momentum equation reduces to:

$$\frac{du_e}{dt}=\frac{1}{L_E}\frac{\Delta P}{\rho}-8\frac{\mu}{\rho}\frac{u_e}{h_T^{\,2}}\frac{L_V}{L_E}. \qquad (3)$$

In addition the pump compliance and forcing terms are obtained by considering conservation of mass in the pump cavity.

$$\frac{d(\rho V)}{dt}=-\rho u_e A_E \qquad (4)$$

Assuming polytropic compression we obtain:

$$\frac{dP}{dt}=-\rho\alpha^2\frac{n}{\gamma}\frac{u_e A_E}{V}-\rho\alpha^2\frac{n}{\gamma}\frac{1}{V}\frac{dV}{dt} \qquad (5)$$

$$\frac{d\rho}{dt}=\frac{\gamma}{\alpha^2 n}\frac{dP}{dt} \qquad (6)$$

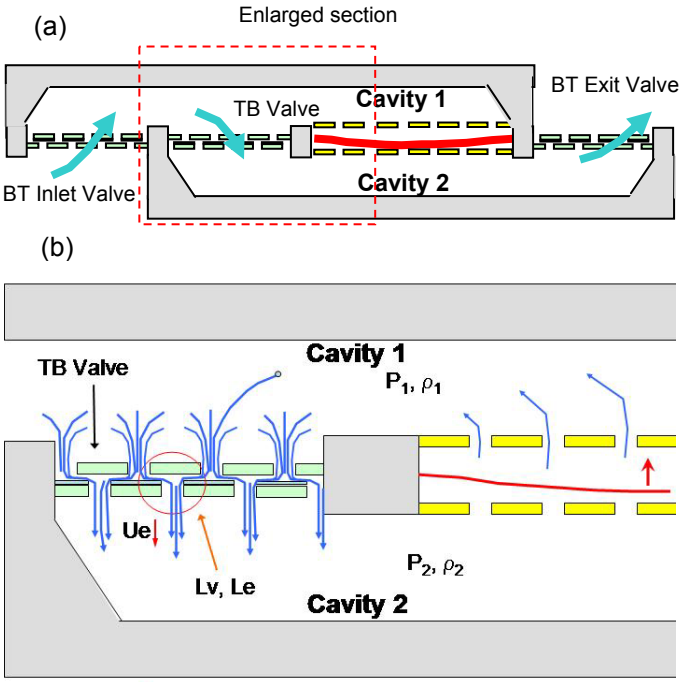

Figure 3. (a) A depiction of a two-stage micro vacuum pump. Gas enters the inlet valve, is compressed in the first cavity, transferred to the second cavity though the top to bottom valve (TB valve), then compresses again and expelled though the exit valve. (b) Equations relating the top and bottom pumping cavities are obtained by taking the line integral of the momentum equation along a streamline through the valve. Pressures and densities are assumed to be uniform in each pumping cavity.

Mass conservation equations for each cavity, and momentum equations for each valve are required. The equations must account for valve open or closed state. Thus the system of equations for the pump is:

$$\frac{du_{e1}}{dt}=\frac{1}{L_E}\frac{(P_1-P_2)}{\rho_1}H_1-8\frac{\mu}{\rho_1}\frac{u_{e1}}{h_T^{\,2}}\frac{L_V}{L_E}H_1 \qquad (7)$$

$$\frac{du_{e2}}{dt}=\frac{1}{L_E}\frac{(P_{inlet}-P_1)}{\rho_{amb}}H_2-8\frac{\mu}{\rho_{amb}}\frac{u_{e2}}{h_T^{\,2}}\frac{L_V}{L_E}H_2 \qquad (8)$$

$$\frac{du_{e3}}{dt}=\frac{1}{L_E}\frac{(P_2-P_{exit})}{\rho_2}H_3-8\frac{\mu}{\rho_2}\frac{u_{e3}}{h_T^{\,2}}\frac{L_V}{L_E}H_3 \qquad (9)$$

$$\frac{dP_1}{dt}=-\rho_1\alpha^2\frac{n}{\gamma}\frac{u_{e1}A_E}{V_1}H_1+ \qquad (10)$$
$$+\rho_{inlet}\alpha^2\frac{n}{\gamma}\frac{u_{e2}A_E}{V_1}H_2-\rho_1\alpha^2\frac{n}{\gamma}\frac{1}{V_1}\frac{dV_1}{dt}$$

$$\frac{dP_2}{dt}=+\rho_2\alpha^2\frac{n}{\gamma}\frac{u_{e1}A_E}{V_2}H_1 \qquad (11)$$
$$-\rho_{exit}\alpha^2\frac{n}{\gamma}\frac{u_{e3}A_E}{V_2}H_3-\rho_2\alpha^2\frac{n}{\gamma}\frac{1}{V_2}\frac{dV_2}{dt}$$

$$\frac{d\rho_1}{dt}=\frac{\gamma}{\alpha^2 n}\frac{dP_1}{dt} \qquad (12)$$

$$\frac{d\rho_2}{dt}=\frac{\gamma}{\alpha^2 n}\frac{dP_2}{dt} \qquad (13)$$

where the subscripts on the velocities refer to: (1) Top to Bottom valve, (2) inlet valve, (3) exit valve. All other numerical subscripts refer to (1) top or (2) bottom pump cavities. The valve position functions, H, allow valves to be turned on or off. H is set to one when the valve is on and zero when off. Logic statements are added to the ODE program code to insure that the valve velocities themselves are set to zero when the valves are closed. Care must be taken to insure that terms associated with velocities have the appropriate density. For example when the velocity through TB valve (valve 1) is from cavity 1 to cavity 2 the density of cavity 1 should be used. Conversely if the velocity becomes negative the density of cavity 2 must be used.

Solutions to this system of equations were found using an ODE solver in Matlab®. Input parameters are the inlet and exit pressure, and the frequency and volume displaced by the membrane motion. Initial conditions for the cavities pressure were chosen consistent with the initial valve configuration, and the initial value of the flow velocity in the valves was assumed zero. The time evolution was then determined assuming a sinusoidal variation of cavity volume with time. The computation was performed until the steady state condition was reached, which for the purposes of the present study was defined as a cycle to cycle variation of the cavity pressure less than 10^{-5} of the overall pump pressure rise. In addition mass conservation during the cycle at steady state conditions was evaluated by comparing the total mass flow through each valve. For the results presented here the mass flow through the three valves agrees with better than 1% error.

3.1 The Viscous Length

The viscous length L_v appearing in Eq. 3 determines the damping of the pump system and accounts for pressure discrepancies between the thermodynamic and dynamic model. As shown in Fig. 3 L_v is associated with viscous effects in the valve. As fluid enters the valve it experiences wall shear, and the fluid core must be accelerated through the different valve sections (i.e. electrodes and gap spaces). Pressure losses associated with these events have been described in detail by *Astle et al*.[1]

In general the viscous length would be a function of valve geometry and frequency of operation. For the present study the Stokes number based in valve gap is small and, therefore, the viscous length at low frequency is used. Thus using equation (3) for steady state conditions gives,

$$\Delta P = \frac{8 \cdot \mu \cdot L_V \cdot u_e}{h_T^2}. \qquad (14)$$

Taking the derivative and solving for L_V gives,

$$L_V = \frac{h_T^2}{8\mu}\frac{d\Delta P}{du_e}. \qquad (15)$$

Equation (15) allows use of the steady pressure loss model previously developed for the "checkerboard" microvalves to determine L_v for a given geometry and flow rate. Figure 4 shows a plot of the pressure loss in the valve as a function of flow rate. The slope of the curve at low flow rate is used to determine the viscous length. The figure shows the slope of ΔP vs. Q to be approximately constant for a range of flow rates typical of these micropumps. The dynamic equations were solved using a constant value of L_v.

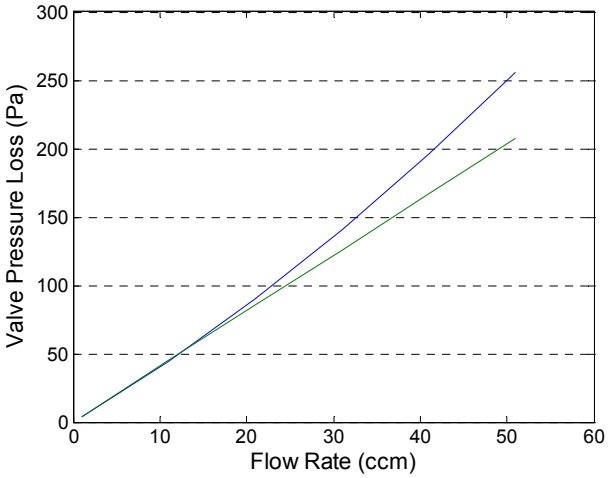

Figure 4. Valve pressure loss vs. flow rate for a typical valve geometry. The slope is used to determine L_V.

As discussed by *Astle et al*,[1] there is an optimum valve geometry for given micropump size constraints. Figure 5 shows that for a given gap between the valve electrodes and a given sealing distance for the membrane and bottom electrode holes, there is an optimum hole size that minimizes pressure losses. If the holes are too large volume flow rates in the electrode/membrane gap (and thus gap velocity and pressure loss) become large. If the electrode holes become too small core acceleration losses are dominant. This minimum pressure loss geometry translates directly into a minimum viscous length L_v. Typical optimum micropump electrode hole sizes are of the order of 20 μm, with electrode gap distances of approximately 4 μm. Sealing distances (the distance between the membrane holes and the bottom, seating, electrode's holes) are of the order of 10 μm. See Fig. 6 for a typical valve geometry cutaway.

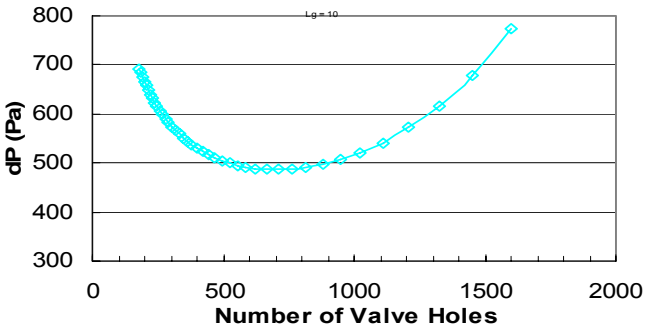

Figure 5. Pressure loss curve for a micropump microvalve. Valve gap height: 4 μm, sealing distance: 10 μm. Minimum pressure loss corresponds to a electrode hole size of ~20 μm and L_v ~ 30 μm.

3.2 The Inertial Length

The inertial length of the microvalve determines the resonant behavior of the pump system. The inertial length can be though of as the equivalent velocity weighted distance the fluid must traverse through the valve. Fig. 6 shows a particle starting at the valve entrance (bottom of the figure) and following a streamline to the exit of the valve. L_E is found by integration of the velocity along a stream line. Namely:

$$L_E = \frac{1}{u_e}\int \vec{u}\cdot d\vec{s} \qquad (16)$$

As is the case for the viscous length, the inertial length is expected to be a function of valve geometry and operating frequency. However the stokes number for present conditions is small and therefore the low frequency value of L_E is used. Thus the value for L_E was obtained using CFD simulations of flow through the microvalve. Fig. 6 shows streamlines from one such simulation. The commercial code Fluent® was used with a laminar 2nd order solver. Typical L_E values obtained using equation (16) are of the order of 200 μm. More accurate predictions may be obtained using unsteady CFD simulations of the flow in the valve. Future work will include development of a model to predict L_E based on geometry and operating frequency.

4 RESULTS

The high frequency performance of the micro pump was determined at conditions corresponding to the two operating points of the micro gas chromatograph. These conditions are summarized in Table1. It should be noted that the dynamic model is for a two stage pump, while the micro gas chromatograph vacuum pump is an 18-stages design. The results reported here were obtained at the same compression ratio, V, and flow rate, Q, as the micro gas chromatograph and, therefore, the overall pressure rise is significantly smaller. In Table 1, operating point 1 corresponds to the analysis operating mode of the chromatograph (low flow rate at high pressure rise) and operating point 2 corresponds to the sampling mode (high flow rate at low pressure rise).

Table 1 Pump Operating Points

	Dynamic Model		μGC	
Operating Point	1	2	1	2
No of Stages	2	2	18	18
P inlet (atm)	0.945	0.975	0.5	0.8
P exit (atm)	1	1	1	1
P_{Vac} (atm)	0.055	0.025	~ 1/2	~ 1/5
V_r	0.95	0.95	0.95	0.95
Desired Q (sccm)	2	25	2	25

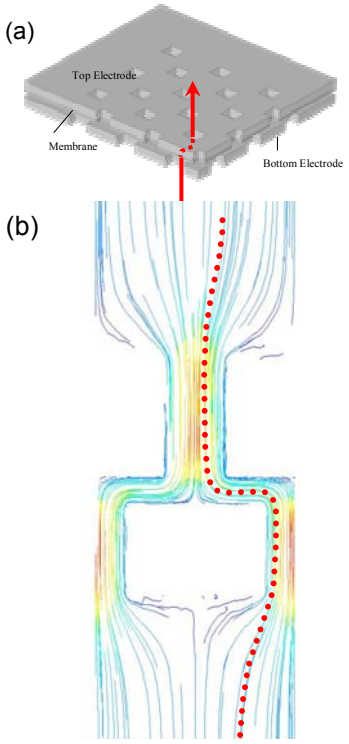

Figure 6. (a) Cutaway of checkerboard microvalve with an arrow indicating flow path and direction. (b) An example streamline on which to find L_E.

The pump geometry used in the present calculations are listed in Table 2. These are typical design values for the micro gas chromatograph vacuum pump. Table 2 also lists the viscous and inertia lengths corresponding to this geometry.

Table 2 Pump Geometry used in Analysis

Cavity Height Hc.	100	μm
Pumping cavity Area	4	mm^2
Pumping Membrane Displacement	7.5	μm
Valve Electrode Gap hg	5	μm
Valve Expected Viscous Length Lv	30	μm
Valve Expected Inertial Length L_E	200	μm

Valve timing is an important consideration in the operation of the pump, particularly at high frequency. A quasi-steady analysis provides a first estimate of the valve opening and closing times. This analysis shows that the valves should open when the pressure in a cavity increases above the pressure in the following cavity, and close when the membrane reaches the end of the stroke, The quasi-steady valve timing values are listed in Table 3. In the calculations reported here it is assumed that the valves open and close at the specified times independent of the pressure in the cavities. Table 3 also lists the optimum valve timing for high frequency operation obtained as described below.

Table 3 Valve timing

	Operating point 1		Operating point 2	
	t_{op}/T BTDC	t_{cl}/T ATDC	t_{op}/T BTDC	t_{cl}/T ATDC
Quasi-steady	0.28	0	0.36	0
High frequency (30 kHz)	0.25	0.11	0.3	0.125

Figure 7 shows calculated pressure and velocity traces for a two stage pump operated at low frequency (100 Hz), and for the pump geometry given in Table 2. Operating point 1 is shown with quasi-steady valve timing. The time origin in Figure 7 corresponds to maximum volume of cavity 1 and minimum volume of cavity 2. For the first part of the cycle ($0 \le t/T \le 0.22$) the valves are closed and the membrane moves towards cavity 1, thus compressing air in it and expanding air in cavity 2. At $t_{op}/T = 0.28$ (note that t_{op} is referenced to TDC as shown in Fig. 2) the TB valve connecting the two cavities opens and the velocity in the valve increases to ~0.05 m/s. The motion of the membrane towards cavity 1 forces air through the valve into cavity 2. When the membranes reaches the end of the stroke, TDC (t/T = 0.5), the valves close and a new compression phase begins. This time the motion of the membrane compresses air in cavity 2 and expands air in cavity 1. At time t/T = 0.72, the inlet and exit valves open and motion of the membrane forces air from cavity 2 to the exit, and draws air from the inlet into cavity 1. At time t/T = 1, the end of the cycle, the valves close and a new cycle begins. As seen in Fig. 7 the velocity in the valves adjusts quickly to the initial pressure imbalance and then is only affected

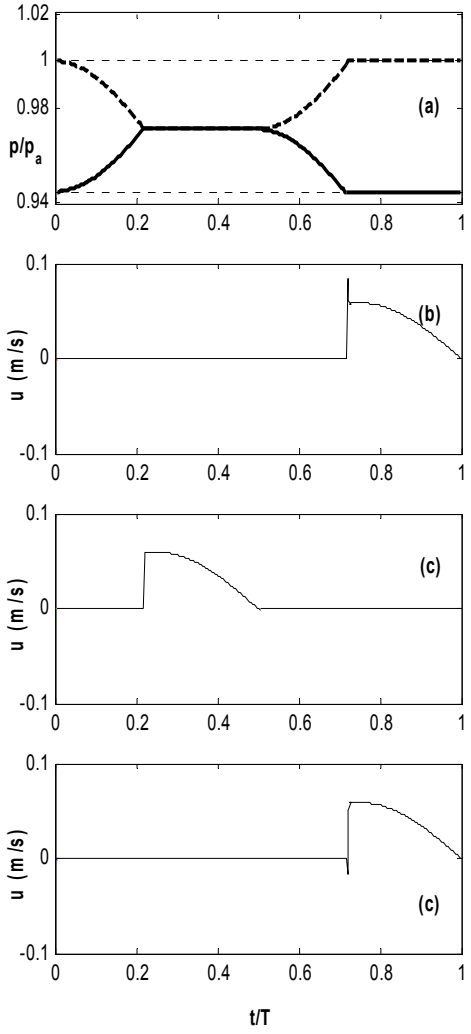

Figure 7. (a) A pressure trace of the top cavity 1 (—) and bottom cavity 2 (--) with quasi-steady valve timing. Pressure in atm is plotted against normalized pump cycle time. Inlet and exit conditions are shown as thin dotted lines. L_V = 30 μm, L_E = 200 μm. f = 100 Hz (b) Exit velocity of the inlet valve. (c) Exit velocity of the TB valve. (d) Exit velocity of the exit valve.

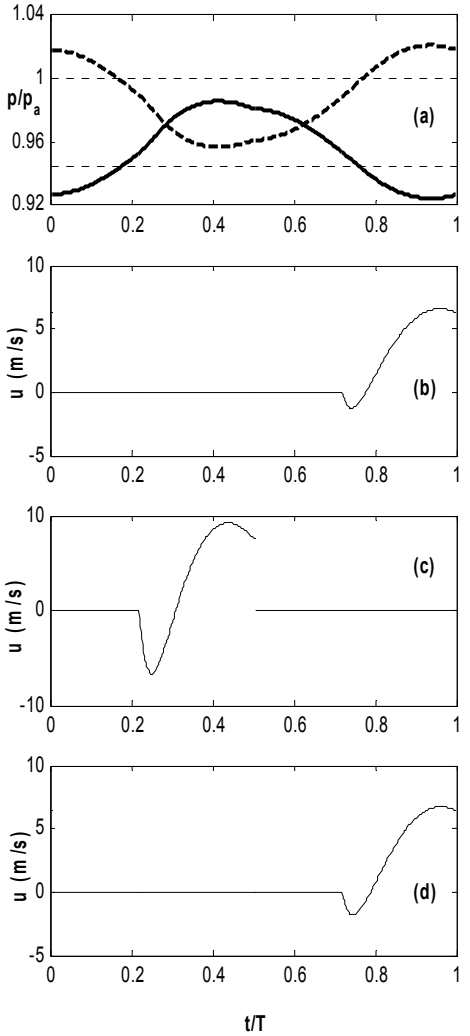

Figure 8. (a) A pressure trace of the top cavity 1 (—) and bottom cavity 2 (--) with the same quasi-steady valve timing as used in Fig. 7. Pressure in atm is plotted against normalized pump cycle time. Inlet and exit conditions are shown as thin dotted lines. Lv = 30 μm, L_E = 200 μm. f = 30 kHz (b) Exit velocity of the inlet valve. (c) Exit velocity of the TB valve. (d) Exit velocity of the exit valve.

by the membrane volume displacement. Transient events are relatively short compared to the cycle period so that dynamic effects are not important.

Figure 8 shows the same pump as in Fig. 7 operated at 30 kHz. Although the same basic pumping process takes place, there are very significant differences. First the pressure in cavity 1 can have values well below the inlet pressure, and the cavity 2 pressure can reach values well above the exit pressure. This is in order to drive the large flow velocity and associated pressure loss during gas transfer. Another feature shown by the pressure trace is that the valves are forced to open well before the cavity pressures have equilibrated. This results in reversed flow through the valve. The valve is then closed at TDC, a time when its velocity is still very large. Pressure and velocity are out of phase with membrane motion. This is shown clearly by comparing the TB valve velocity in this case with the results at low frequency (Fig. 7).

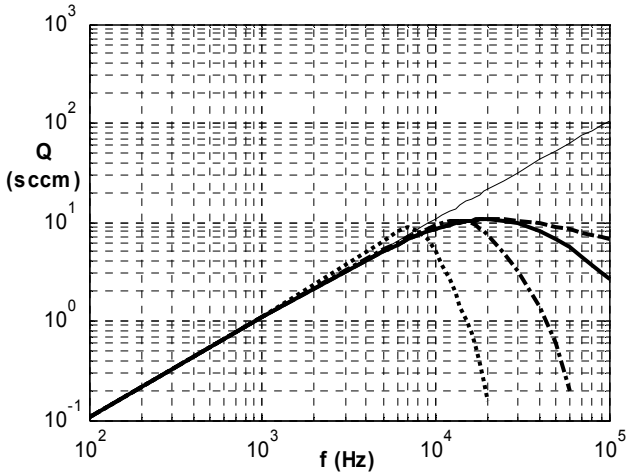

Figure 9. Flow rate vs frequency for L_E = 50 (--), 200 (—), 1000 (-.-), 5000 (..) μm and a constant Lv = 30 μm. The ideal thermodynamic flow rate is represented by a thin straight line. Valve timing is quasi-steady, operating point 1 (see Table 1).

Figures 9 through 12 show typical performance curves of the micropump for varying inertia and viscous lengths, and valve timing. In these plots the thick solid line is the flow rate as function of frequency for the L_V and L_E values expected for the micropump listed in Table 2 and quasi-steady valve timing. The thermodynamic model of Astle *et al*[1] predicts a linear increase of flow rate with frequency. This result is also shown in the figures and is labeled the ideal thermodynamic flow rate. These results show that the flow rate closely follows that ideal value up to a frequency of the order of 10 kHz where the dynamic effects discussed above limit the performance of the pump. For the present design the maximum flow rate is 10 sccm for operating point 1.

The inertial and viscous lengths play an important role in the performance of the micropump. Figure 9 shows how inertial length affects the flow rate as a function of frequency. Low values of inertial length produce the best performance. At moderate values of L_E there are very small differences in flow rate up to frequencies close to the resonant frequency. For very large L_E there is some improvement over the ideal thermodynamic flow rate. However, the cutoff frequency and overall flow rate are lower. These trends suggest that targeting a small value of L_E will lead to better performance. Figure 9 also shows that L_E affects the location of the resonant peak.

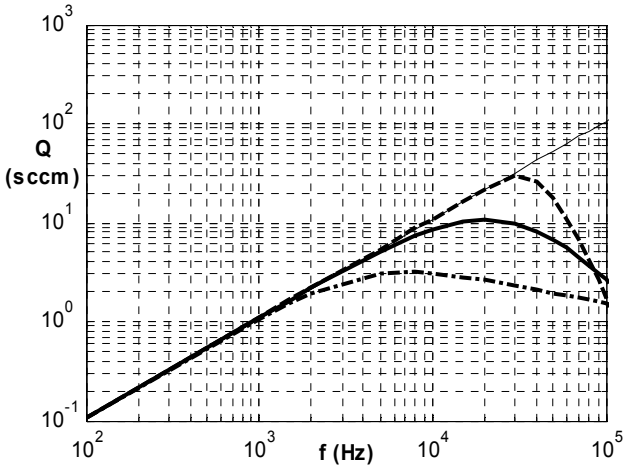

Figure 10. Flow rate vs frequency for L_V = 10 (--), 30 (—), 50 (-.-) μm and a constant L_E = 200 μm. The ideal thermodynamic flow rate is represented by a thin straight line. Valve timing is quasi-steady, operating point 1 (see Table 1).

It is interesting to compare the resonant frequency of the pump with that of an acoustic resonator of similar size given by the equation,[6]

$$f_o = \frac{\alpha}{2\pi}\sqrt{\frac{A_E}{L_E V_c}} \qquad (18)$$

For the present pump cavity volume f_o is calculated to be 62 kHz. This is almost double what the dynamic model predicts for the nominal L_E = 200 μm case. Discrepancies may arise from pump discharge from cavity to cavity, and from cavity to ambient conditions during different portions of the pump cycle. Using a combined top and bottom cavity volume in equation (18), f_o becomes 44 kHz. These results suggest that the small cavity volume typical of micropumps allows the resonant frequency to be in the frequency range (~10 – 100 kHz) needed for the μGC pump.

The viscous length also has an important effect on pump performance. Figure 10 shows that smaller L_V translates into larger flow rate for a given operating condition. The figure also shows that L_V affects the frequency for maximum performance of the pump. Currently the L_V minimum is about 30 μm for typical optimized microvalves (see Table 2). Valve pressure drop decreases quickly as electrode gap separation increases. This implies that L_V will also decrease dramatically with electrode gap separation distance. Technologies are being developed to increase the electrode gap separation distance while maintaining acceptable drive voltage.

The effect of valve timing is documented in Figures 11 and 12. Figure 11 shows that for quasi-steady timing the maximum flow rates is achieved when the pressures

are matched before the TB valve opens. Resonance location seems only weekly affected by changes in opening time t_{op}. It should be noted that valve opening time does not affect performance at low frequency. Valve closing time has a much greater impact on flow rate than valve opening time. Figure 12 shows that as closing time is increased past TDC the flow rate increases. However, there is an optimal value beyond which the flow rate decreases. It is also interesting to note that as valve closing time gets farther from TDC the flow rate deviates farther from the thermodynamic model even at low frequencies. Valve close time also plays a role in shifting the resonance frequency as expected.

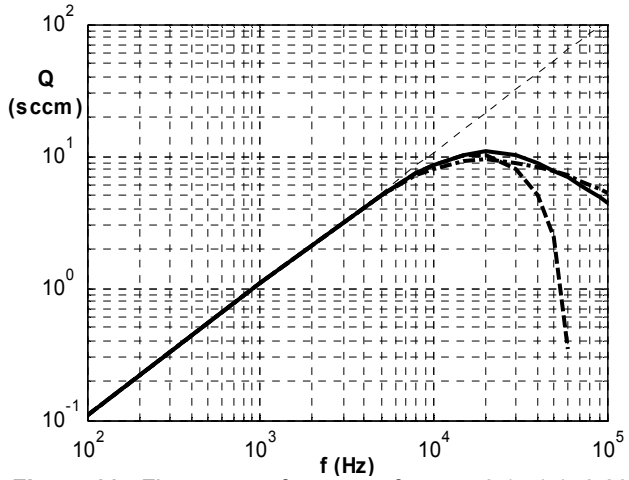

Figure 11. Flow rate vs frequency for t_{op} = 0.15 (--), 0.28 (—), 0.35 (-.-) t/T before TDC and a constant t_{cl} = 0 t/T after TDC. The ideal thermodynamic flow rate is represented by a thin straight line. L_E = 200 μm L_V = 30 μm, Operating point 1 (see Table 1).

The results shown in Figs. 11 and 12 suggest that there is a "high frequency" timing that will provide maximum flow rate at the resonant frequency. Figure 13 is a map of the flow rate and TB valve velocity at closing as a function of valve opening and closing times at the resonant frequency of 30 kHz. The point of maximum flow corresponds to where the exit velocity of the TB valve is zero at valve close (12.8 sccm at t_{op}/T of 0.25 and t_{cl} /T of 0.11). The ~12 sccm at the optimum operating conditions is significantly larger than the required 2 sccm for the μGC. Therefore a smaller volume displacement can be used, reducing required driving voltage. Figure 14 shows a similar map of the flow rate and the mechanical power used by the membrane motion. The results show that the maximum flow rate does not correspond directly to peak mechanical power. They suggest, however, that reducing the compression period increases the required power.

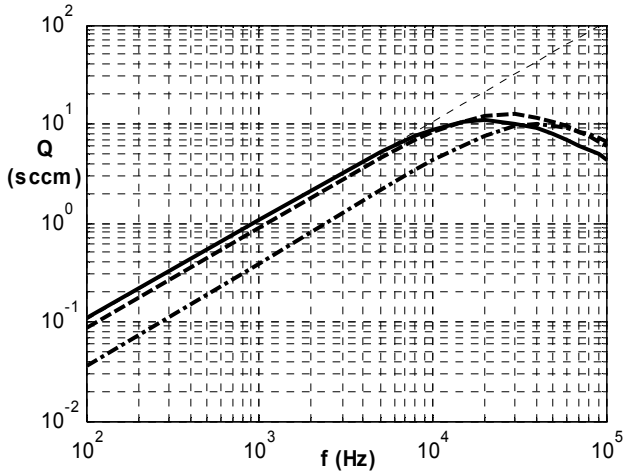

Figure 12. Flow rate vs frequency for t_{cl} = 0 (--), 0.11 (—), 0.22 (-.-) t/T after TDC and a constant t_{op} = 0.28 t/T before TDC. The ideal thermodynamic flow rate is represented by a thin straight line. L_E = 200 μm L_V = 30 μm, Operating point 1 (see Table 1).

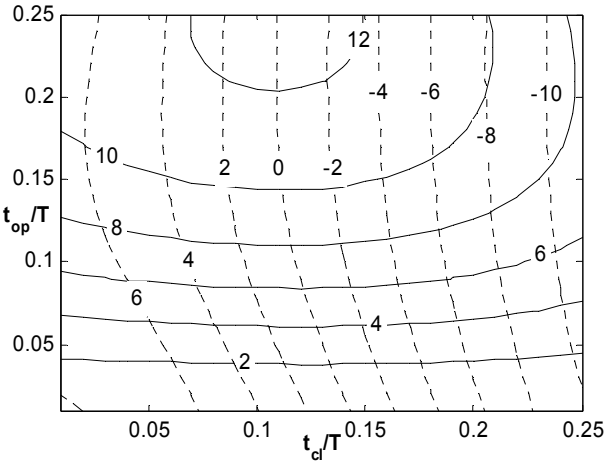

Figure 13. Flow rate (sccm) (—) and TB valve final exit velocity (m/s) (--) for variation in t_{op}/T before TDC and t_{cl} /T after TDC. L_E = 200 μm L_V = 30 μm, f = 30 kHz (resonance), Operating point 1 (see Table 1).

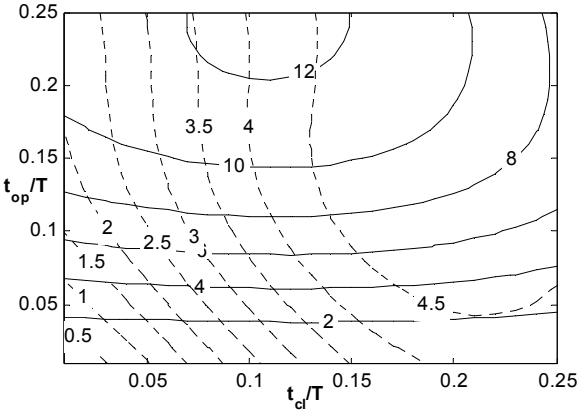

Figure 14. Flow rate (sccm) (—), and required pump power (mW) (--) for variation in t_{op}/T before TDC and t_{cl} /T after TDC. L_E = 200 μm L_V = 30 μm, f = 30 kHz (resonance), Operating point 1 (see Table 1).

Figure 15 shows the mechanical power at the optimum high-frequency timing as a function of frequency. The plot also shows the mechanical power computed using the ideal thermodynamic model. As expected, required power is larger than the thermodynamic power since the present dynamic model includes viscous dissipation in the valves. The difference increases with frequency.

Figure 16 shows pressure and velocity traces for the pump operating at resonance and with high-frequency-optimized valve timing. Optimum valve timing implies that the TB valve exit velocity is zero when the valve is actuated closed. However, the inlet and exit valves do not reach this velocity condition due to their different conditions. This effect may be reduced when more than two pump cavities are used since the exit valve to the two stage pump would become the TB valve for the next set of cavities and would experience similar pressure differences as the TB valve of the first two cavities. This suggests that the TB valve timing is the best to optimize for multistage pumps. Fig. 16 shows that the pressures are not matched and there is an initial negative velocity through the valve. This timing, however, does correspond to the maximum flow rate.

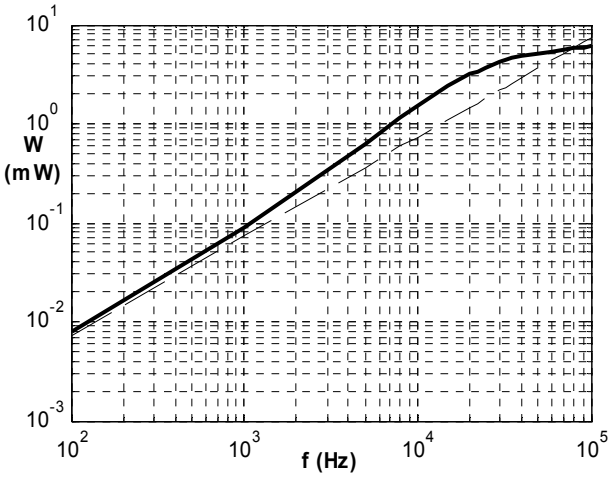

Figure 15. Required pump power (—), and thermodynamic pump power (--) vs. frequency for ideal high frequency timing obtained from Fig. 13. L_E = 200 μm L_V = 30 μm, Operating point 1 (see Table 1).

The pump must also match the second operating point consisting of a high flow rate (25 sccm) and low pressure differential (1/5 atm). Figure 17 shows the flow rate as a function frequency for the optimum high-frequency valve timing. Resonance for the second operating point was reached at approximately 35 kHz, with a maximum flow rate of ~21 sccm. This is slightly less than the require flow rate and small adjustments of the cavity volume would be needed to obtain the required performance. The mechanical power of operating point 2 as a function of frequency is shown in Figure 18. The results show a larger power requirement compared to the first operating point and an increase relative to the thermodynamic power near resonance, a similar trend as that of the first operating point (Fig. 15). It is also larger than that of the first operating point.

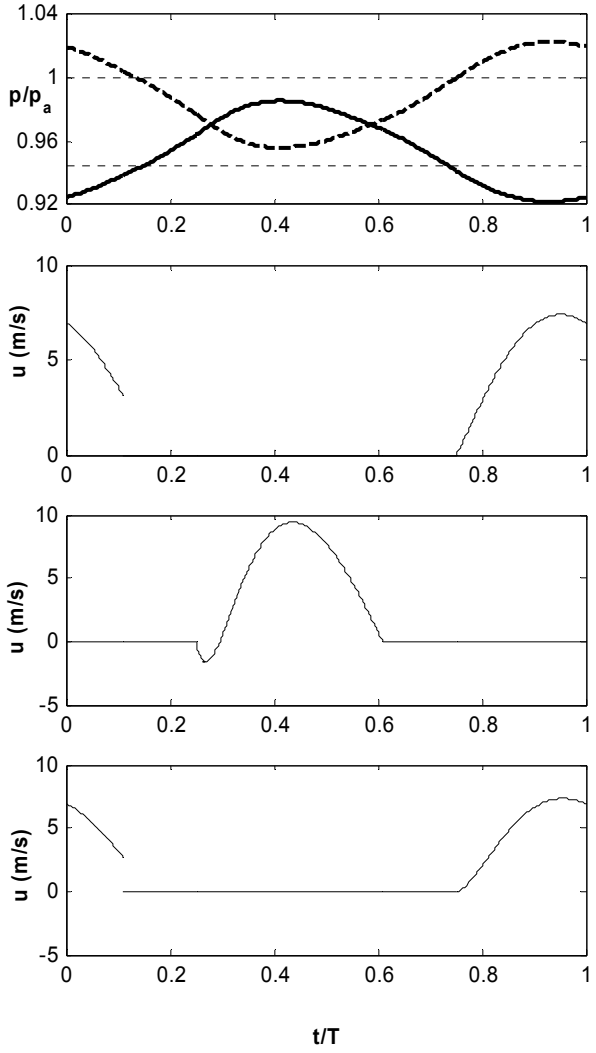

Figure 16. (a) A pressure trace of the top cavity 1 (—) and bottom cavity 2 (--) with high frequency valve timing. Pressure in atm is plotted against normalized pump cycle time. Inlet and exit conditions are shown as thin dotted lines. Lv = 30 μm, L_E = 200 μm. f = 30 kHz (b) Exit velocity of the inlet valve. (c) Exit velocity of the TB valve. (d) Exit velocity of the exit valve.

5 CONCLUDING REMARKS

A dynamic model of micro pumps has been developed to determine the performance of a μGC vacuum pump at high frequency. The results of this model are compared to the results a previously developed thermodynamic model of an ideal pump. At low frequencies the two models are in good agreement. The major differences in performance come from viscous losses and inertial effects in the pump cavities and microvalves. These are modeled in the dynamic equations in terms of an effective viscous and inertial length which are determined using a CFD model to be of the order of 30 μm and 200 μm, respectively for a typical microvalve.

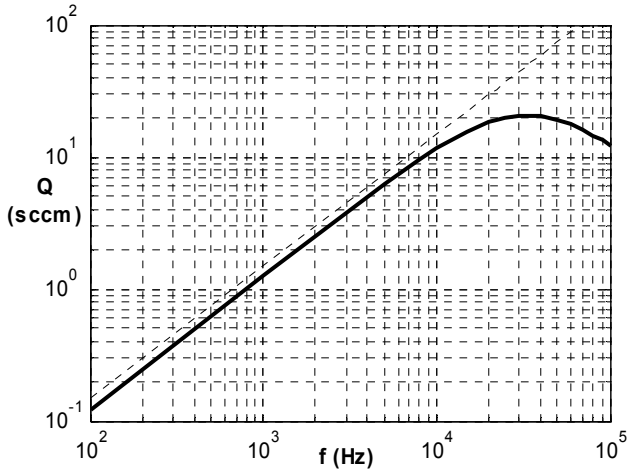

Figure 17. Flow rate vs frequency for high frequency valve timing (—). The ideal thermodynamic flow rate is represented by a thin dashed line. L_E = 200 μm L_V = 30 μm, Operating point 2 (see Table 1).

Maximum pump performance was obtained near the resonant frequency of the pump system. At resonance the valve timing was out of phase with the pump membrane motion. Highest flow rates were obtained when the TB valve exit velocity was zero as the valve was closed. At resonance this meant that valves were open for part of the compression cycle of the following cavity. Inlet and exit valves did not have zero velocity when closed. Multistage pumps effectively see many similar TB valves with one inlet and one exit valve. This means that for a multistage pump optimization of the TB valves is a higher priority than the inlet and exit valves. The resonance frequency for the micropump was much lower than that predicted by acoustic resonator theory. This is thought to be due to cavity-cavity interaction which results in large differences in cavity volumes and exit conditions during different portions of the pump cycle.

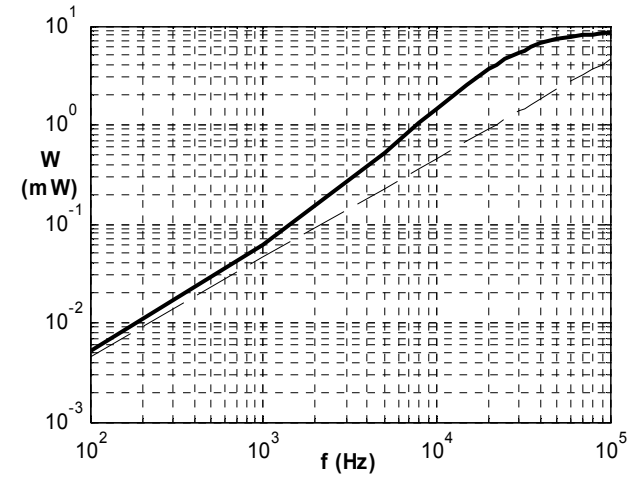

Figure 18. Power vs frequency for high frequency valve timing (—). The ideal thermodynamic flow rate is represented by a thin dashed line. L_E = 200 μm L_V = 30 μm, Operating point 2 (see Table 1).

Power consumption predicted by the dynamic micropump model give higher values than those calculated using the ideal thermodynamic model because of viscous losses. Power required also increases near the pumps resonant frequency.

Dynamic analysis of the micro vacuum pump, show that it is feasible to meet the micro gas chromatograph's operating requirements with the proposed pump design. However, in order to achieve required pressures and flow rates it is important to limit internal viscous and other loss mechanisms. For example operation of the system at frequencies as large as 50kHz is realizable. Optimizing parameters such as valve timing, driving frequency, volume ratio and resonance frequency is critical to provide the required flow rate and pressure rise at the two operating points of the pump.

ACKNOWLEDGMENTS

This work made use of Engineering Research Centers Shared Facilities supported by the National Science Foundation under Award Number EEC-0096866.

REFERENCES

[1] Astle A., A. Paige, L. P. Bernal, J. Munfakh, H. Kim, K. Najafi, "Analysis and design of multistage electrostatically-actuated micro-vacuum pumps," Proceedings of 2002 ASME International Mechanical Engineering Congress, Noverber 17-22, New Orleans, LA, Paper number IMECE2002-39308.

[2] Zegerle, R. & Sandmier, H. 1996 *Microfluidics*, Proc. Seventh International Symposium on Micro Machine and Human Science, pp 13 – 20, IEEE.

[3] Koch, M, Harris, N, Evans, A, White, N & Brunnschweiler, *A novel micromachined pump based on thick film piezoelectric actuation*, **Transducers '97**, 1997 International Conference on Solid-State Sensors and Actuators, Chicago, June 16-19, 1997.

[4] Stehr, M, Gruhler, H, Straatmann, H, Messner, S, Sandmaier, H & Zengerle, R, *The selfpriming VAMP*, **Transducer '97**, 1997 International Conference on Solid-State Sensors and Actuators, Chicago, June 16-19, 1997.

[5] Wijngaart, W., Andersson, H., Enoksson, P., Noren, K. & Stemme, G. 2000 *The first self-priming and bi-directional valve-less diffuser micropump for both liquid and gas*, Proc. 13th Annual International Conference on Micro Electro Mechanical Systems, MEMS 2000, pp 674-679.

[6] Müller, M.O., Bernal, L.P., Washabaugh, P.D., Moran R.P., Parviz, A.B. & Najafi, K. 2002 *Micromachined Acoustic Resonators for Microjet Propulsion*, AIAA 2000-0547.

[7] Müller, M.O., Bernal, L.P., Washabaugh, P.D., Moran R.P., Parviz, A.B. & Najafi, K. 2002 *Thrust Performance of Micromachined Synthetic Jets*, AIAA 2003-2404.

[8] Müller, M.O., Bernal, L.P., Washabaugh, P.D., Kim, H.S. & Najafi, K. 2002 *Resonance Effects of Electrostatically Actuated Acoustic Jets*, AIAA 2003-1272.